JCTC Journal of Chemical Theory and Computation

Article

pubs.acs.org/JCTC

The Frozen Cage Model: A Computationally Low-Cost Tool for Predicting the Exohedral Regioselectivity of Cycloaddition Reactions Involving Endohedral Metallofullerenes

Marc Garcia-Borràs,[†] Adrian Romero-Rivera,[†] Sílvia Osuna,[‡] Josep M. Luis,*[,†] Marcel Swart,*[,†,§] and Miquel Solà*[,†]

[†]Institut de Química Computacional and Departament de Química, Universitat de Girona, Campus Montilivi, 17071 Girona, Catalonia, Spain

[‡]Department of Chemistry and Biochemistry, University of California, Los Angeles, 607 Charles E. Young Drive, Los Angeles, California 90095, United States

[§]Institució Catalana de Recerca i Estudis Avançats (ICREA), Pg. Lluís Companys 23, 08010 Barcelona, Catalonia, Spain

Supporting Information

ABSTRACT: Functionalization of endohedral metallofullerenes (EMFs) is an active line of research that is important for obtaining nanomaterials with unique properties that might be used in a variety of fields, ranging from molecular electronics to biomedical applications. Such functionalization is commonly achieved by means of cycloaddition reactions. The scarcity of both experimental and theoretical studies analyzing the exohedral regioselectivity of cycloaddition reactions involving EMFs translates into a poor understanding of the EMF reactivity. From a theoretical point of view, the main obstacle is the high computational cost associated with this kind of studies. To alleviate the situation, we propose an approach named the frozen cage model (FCM) based on single point energy calculations at the optimized geometries of the empty cage products. The FCM represents a fast and computationally inexpensive way to perform accurate qualitative predictions of the exohedral regioselectivity of cycloaddition reactions in EMFs. Analysis of the Dimroth approximation, the activation strain or distortion/interaction model, and the noncluster energies in the Diels–Alder cycloaddition of *s-cis*-1,3-butadiene to X@D_{3h}-C_{78} (X = Ti_2C_2, Sc_3N, and Y_3N) EMFs provides a justification of the method.

INTRODUCTION

The synthesis and characterization of endohedral metallofullerenes (EMFs) nowadays represents one of the most active areas of research in fullerene chemistry. EMFs have interesting physicochemical properties with many potential interesting applications in various fields such as biomedicine (radioimmunotherapy and magnetic resonance imaging contrast agents), energy (solar cells), and electronics (magnetism, superconductivity, and nonlinear optical properties).[1−4]

Organic functionalization of these species is an important research direction for the synthesis of novel EMFs with finely tuned properties. Since the synthesis of the first exohedral adduct of an EMF ($La@C_{82}$) in 1995,[5] great efforts have been devoted to the functionalization of EMFs and to getting a better understanding of their reactivity. Special attention has been paid to cycloaddition reactions such as Diels–Alder (DA), 1,3-dipolar, and Bingel–Hirsch cycloadditions, among others.[3,4] Even so, experimental studies of regioselectivity in cycloaddition reactions to EMFs are still scarce. Two main reasons account for this situation: first, the low production yield[2] and, second, the complexation of the metallic species with the cage that hinders the isolation of sufficient quantities to investigate their reactivity. As a result, the role of the encapsulated cluster in the regioselectivity of these addition reactions is not fully understood yet.[3] In this sense, the current situation in the research of EMFs resembles that of empty cages in 1993 when few reactions involving fullerenes were known. Hirsch in his renowned review[6] wrote referring to fullerene research at that time that, "After the "reign" of the physicists and physical chemists, it now appears to be the time of the preparative chemists."

Some authors consider that the paucity of theoretical studies devoted to the regioselectivity in EMFs contributes to the lack of a clear understanding of the reactivity of EMFs.[7] Quantum mechanical calculations have proven to be extremely useful for experimental chemists especially when it comes to assigning the site of addition in a given adduct based on experimental ^{13}C NMR or UV–vis studies.[8] At the same time, theoretical studies provide valuable hints to understanding the effect of the encapsulated cluster on the regioselectivity of EMFs.[9,10] Most theoretical studies published to date analyze the stability of the different adducts and discuss the regioselectivity of EMFs based on the initial EMF bond lengths, pyramidalization angles, molecular orbitals, electrostatic potential, atomic charges, and Fukui functions (see ref 9 for a review), and only a few theoretical studies are available that make a full thermodynamic and kinetic analysis of the reactivity of all distinct bonds in a given EMF.[11−13] These studies have shown that both the chemical reactivity and regioselectivity are strongly affected by the nature of the incarcerated species. Joint experimental and computational studies are likely to be crucial to advancing the future knowledge of EMF reactivity.

Received: January 24, 2012
Published: March 15, 2012

   dx.doi.org/10.1021/ct300044x | *J. Chem. Theory Comput.* 2012, 8, 1671−1683

The main reason for the scarcity of computational studies devoted to EMF regioselectivity analysis is twofold. First, the number of different bonds that have to be treated for a full analysis of EMF regioselectivity is, with few exceptions, quite large, especially for low symmetry EMFs or if the cluster in the EMF can move freely.[14] Second, calculation of reliable reaction energies and energy barriers requires the use of generalized gradient approximation (GGA), meta-GGA, or hybrid density functional methods including dispersion corrections[15] that for systems of the size of common EMFs is substantially CPU time consuming. On the other hand, simplified methodologies such as the ONIOM method,[16] which was applied to analyze the reactivity of empty cages,[15,17] cannot be generally used in EMFs since all bonds have to be studied with the same defined fragments to make comparisons possible. Moreover, the metallic cluster interacts with different parts of the fullerene and, therefore, it is not possible to clearly partition the fullerene in parts that can be treated at high and low levels of theory.

To reduce the high computational cost of regioselectivity studies in EMFs, some authors propose to make first a thermodynamic analysis of all possible addition sites and then perform a search for the transition states (TSs) of only a reduced number of bonds corresponding to the most favorable additions from a thermodynamic point of view.[9] In this work, our aim is to move one step forward in two directions. First, we demonstrate that the linear Dimroth[18] approximation connecting thermodynamic and kinetic results works for the DA cycloaddition of *s-cis*-1,3-butadiene to X@D_{3h}-C_{78} (X = ∅, Ti_2C_2, Sc_3N, and Y_3N) EMFs. This justifies the use of the thermodynamic study to select the most reactive sites of EMFs. Second, we show that the thermodynamic analysis can be carried out at the frozen geometry of the empty cage adducts. This approach, referred as the frozen cage model (FCM), requires only single point energy calculations and, consequently, saves a lot of CPU time and makes large EMF regioselectivity studies affordable. The goal of the frozen cage model is not obtaining very accurate reaction energies, but selecting the most reactive fullerene bonds at a very low computational cost.

COMPUTATIONAL DETAILS

All density functional theory (DFT) calculations were performed with the Amsterdam Density Functional (ADF) program.[19,20] The molecular orbitals (MOs) were expanded in an uncontracted set of Slater type orbitals (STOs) of single-ζ (SZ), double-ζ (DZ, DZP), and triple-ζ (TZP) quality, with the DZP and TZP basis sets containing diffuse functions and including one set of polarization functions. In order to reduce the computational time needed to carry out the calculations, the frozen core approximation has been used.[19] In this approximation, the core density is obtained and included explicitly, albeit with core orbitals that are kept frozen during the self-consistent field (SCF) procedure. Thus, in this work core electrons (1s for second period, 1s2s2p for third and fourth periods, 1s2s2p3s3p4s3d for fifth period) were kept frozen during the geometry optimizations.[19] An auxiliary set of s, p, d, f, and g STOs was used to fit the molecular density and to represent the Coulomb and exchange potentials accurately for each SCF cycle.[21] Energies and gradients were calculated using the local density approximation (Slater exchange and VWN correlation[22]) with nonlocal corrections for exchange (Becke88)[23] and correlation (Perdew86)[24] included self-consistently (i.e., the BP86 functional). For a proper comparison with the previous studies,[11,12] scalar relativistic corrections have been included self-consistently using the zero order regular approximation (ZORA).[25] All energies reported here have been obtained with the different basis sets in single point energy calculations at geometries that were obtained with the DZP basis (i.e., BP86/DZP). These geometries are taken from our previous studies,[11−13] where all products and TS structures were correctly characterized at the BP86/DZP level of theory. In the present work, we use these optimized structures, and only in some cases we reoptimize the metallic clusters inside the cages but keeping frozen the fullerene cage. Reported energies are obtained at the BP86/TZP//BP86/DZP level, except where otherwise noted.

The actual geometry optimizations were performed with the QUILD[26] (QUantum regions Interconnected by Local Descriptions) program, which functions as a wrapper around the ADF program. The QUILD program constructs all input files for ADF, runs ADF, and collects all data; ADF is used only for the generation of the energy and gradients. Furthermore, the QUILD program uses improved geometry optimization techniques, such as adapted delocalized coordinates[27] and specially constructed model Hessians with the appropriate number of eigenvalues.[27]

RESULTS AND DISCUSSION

In this section we make an exhaustive analysis of the DA cycloadditions of *s-cis*-1,3-butadiene to all nonequivalent bonds of X@D_{3h}-C_{78} (X = ∅, Ti_2C_2, Sc_3N, and Y_3N) EMFs. In carbon cages, there are six possible different C−C bond types A−F (represented in Figure 1), where types E and F are not present

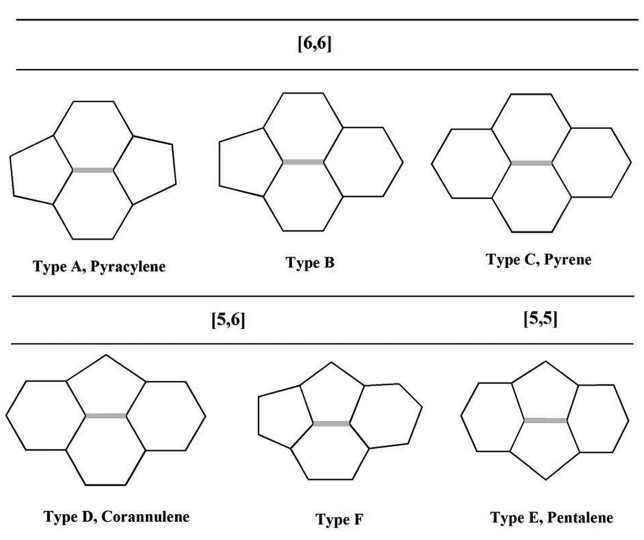

Figure 1. Representation of the different [6,6], [5,6], and [5,5] bond types that may be present in any fullerene structure.

in isolated pentagon rule (IPR) structures.[28] In the particular case of the IPR D_{3h}-C_{78} cage, there are 13 nonequivalent bonds that in this work have been labeled as shown in Figure 2.

The results of this section are presented as follows. First, we discuss in subsection A the fulfillment of the linear Dimroth approximation that relates thermodynamics and kinetics in a set of reactions. Second, in subsection B we analyze the role of the distortion energy in the studied reactions. Third, in subsection C we examine the use of the so-called noncluster model to better understand regioselectivity in these cycloadditions.

dx.doi.org/10.1021/ct300044x | J. Chem. Theory Comput. 2012, 8, 1671−1683

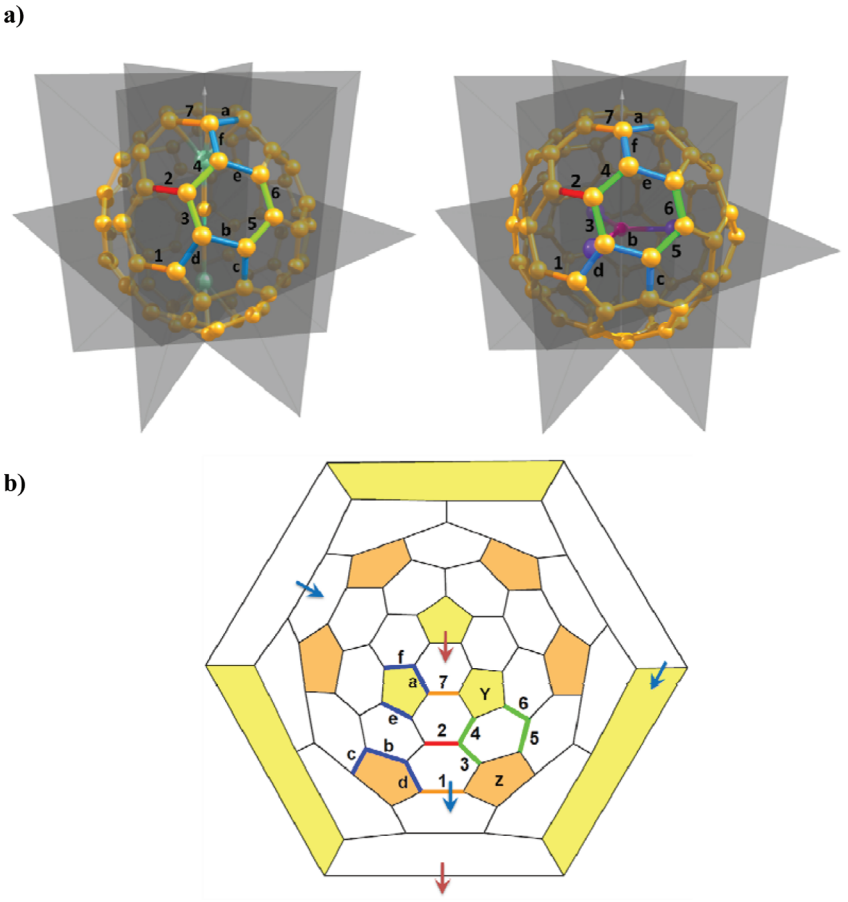

Figure 2. (a) Representation of different nonequivalent bonds of X@D_{3h}-C_{78} (X = Ti_2C_2, left; X = Sc_3N, right), where numbers denote [6,6] bonds and lowercase letters denote [5,6] bonds. Different colors are used to mark the different bond types (orange, type A; green, type B; red, type C; blue, type D). (b) Schlegel diagram of X@D_{3h}-C_{78} (X = Ti_2C_2 and X = Sc_3N), which converts the three-dimensional fullerene structure into a two-dimensional representation. The positions of the titanium atoms facing the different bonds in Ti_2C_2@D_{3h}-C_{78} are symbolized by a red arrow, while blue arrows are used to indicate the positions of scandium atoms in Sc_3N@D_{3h}-C_{78}. The two types of nonequivalent five-membered rings are marked in yellow for type Y (formed by a, f, f, e, and e bonds), and orange for type Z (formed by c, b, b, d, and d bonds).

Finally, the frozen cage model (FCM) is presented in subsection D and justified on the basis of the results of subsections A−C.

A. Fulfillment of the Linear Dimroth Approximation to the Marcus Thermodynamic Treatment: A Thermodynamic Model. Thermodynamic models are normally used to conceptually understand the reaction energies or the activation energies of a reaction. As can be seen in Figure 3, by using a set of two parabolic functions (one for reactants and one for products), we can represent the TS structure on the intersection point between these two functions, that is, the point where the reactant bond dissociation curve intersects with the product bond dissociation parabola.[29]

Marcus based his thermodynamic treatment of the activation free energy for electron-transfer reactions (eq 1) on this parabolic curve model, and where reaction barriers ($\Delta G^{\ddagger}$) are interpreted in terms of intrinsic barriers ($\Delta G_0^{\ddagger}$) for a reference thermoneutral ($\Delta G_{rxn} = 0$) reaction and the energy of reaction (ΔG_{rxn}).[30] Simplifying this equation, and using electronic energies instead of free energies, one can obtain the expression given in eq 2, which is also based on the empirically determined relationship $\Delta\Delta E^{\ddagger} = (1/2)\Delta\Delta E_{rxn}$ given by Dimroth,[18] Brønsted,[31] and Bell, Evans, and Polanyi (BEP).[32] This approximation can be satisfactorily applied when the studied reaction is not too exothermic.

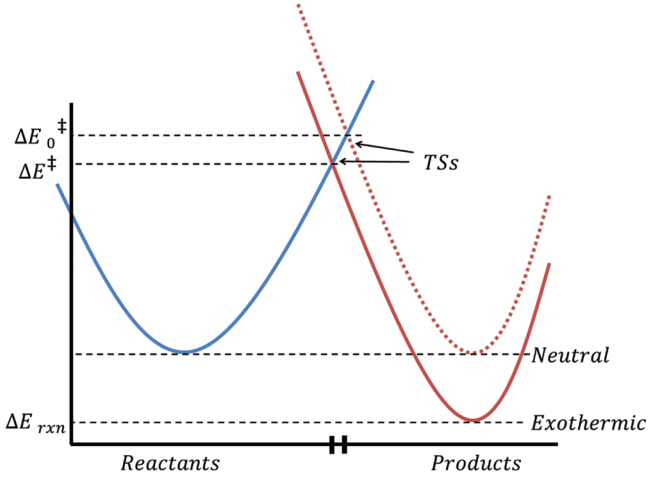

Figure 3. Curve crossing representation of the Marcus thermodynamic treatment.

$$\Delta G^{\ddagger} = \Delta G_0^{\ddagger} + \frac{1}{2}\Delta G_{rxn} + \frac{\Delta G_{rxn}^{\ 2}}{16\Delta G_0^{\ddagger}} \quad (1)$$

dx.doi.org/10.1021/ct300044x | J. Chem. Theory Comput. 2012, 8, 1671−1683

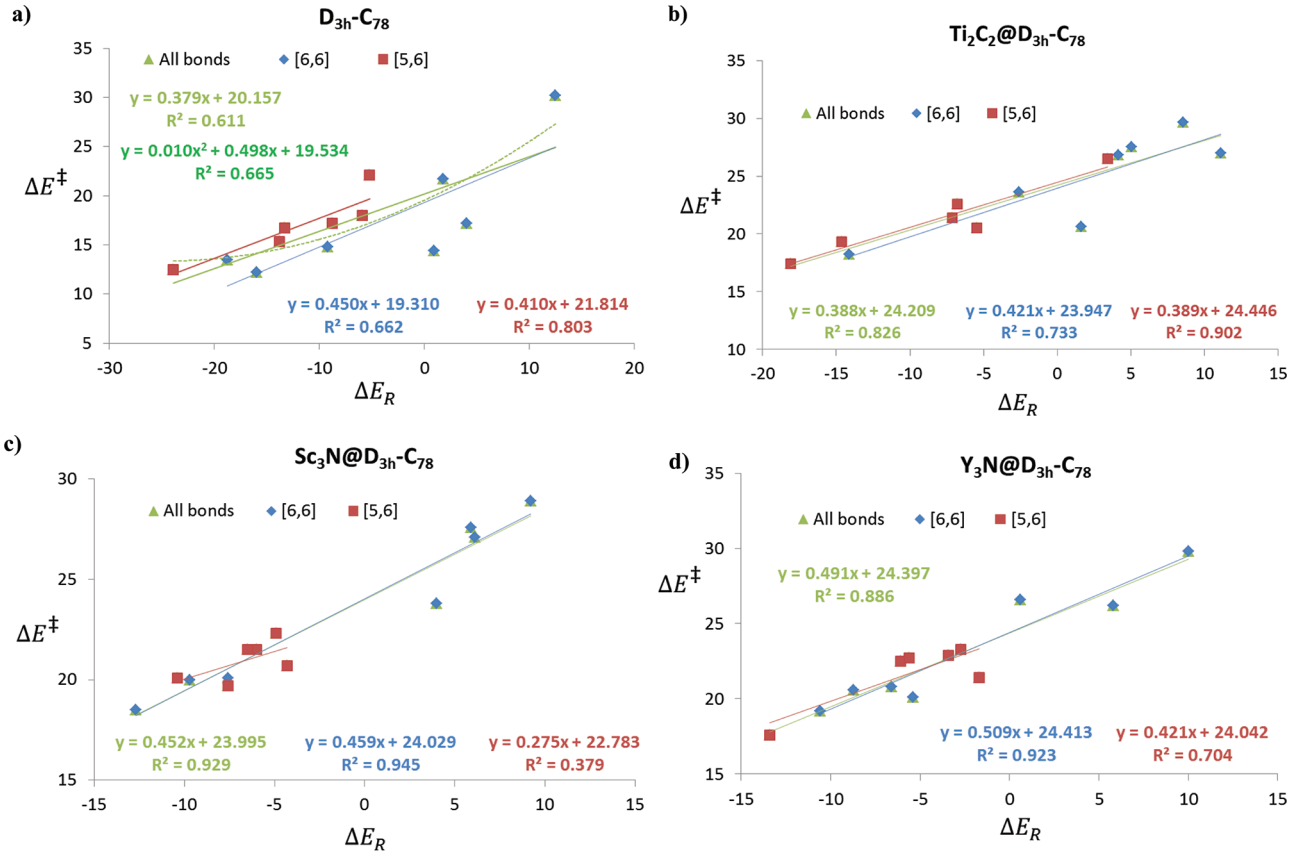

Figure 4. Plot of BP86/TZP//BP86/DZP energy barriers ($\Delta E^{\ddagger}$, kcal·mol^{-1}) versus reaction energy (ΔE_R, kcal·mol^{-1}) for the Diels–Alder reaction of *s-cis*-1,3-butadiene (green) with (a) free D_{3h}-C_{78}, (b) Ti_2C_2@D_{3h}-C_{78}, (c) Sc_3N@D_{3h}-C_{78}, and (d) Y_3N@D_{3h}-C_{78}. We have also represented the two different bond types [6,6] (in blue) and [5,6] (in red).

$$\Delta E^{\ddagger} = \Delta E_0^{\ddagger} + \frac{1}{2}\Delta E_{rxn} \qquad (2)$$

In Figure 4a, energy barriers versus reaction energies for the DA cycloaddition reaction between free D_{3h}-C_{78} and *s-cis*-1,3-butadiene for all nonequivalent bonds are plotted. Although a linear fitting gives a small correlation coefficient, the second order polynomial fitting does not improve significantly the correlation (for a linear fitting R^2 is 0.611; for a second order polynomial curve R^2 is 0.665), which means that the linear Dimroth approximation is as good as the Marcus curve for this studied case.

DA cycloadditions on Ti_2C_2, Sc_3N, and Y_3N@C_{78}:5 ($D_{3h'}$) EMFs are less exothermic than on free C_{78}:5 ($D_{3h'}$), as expected from the fact that EMFs are usually less reactive than their free cages. Thus, we have studied the same correlation for the DA reaction between *s-cis*-1,3-butadiene and all nonequivalent bonds of X@D_{3h}-C_{78} (X = Ti_2C_2, Sc_3N, Y_3N) (see Figure 4b–d). In all cases, reasonable correlations are found for linear fittings (R^2 compressed between 0.758 and 0.929). The adjusted least-squares lines give slopes close to 1/2, which is the expected value given by the Dimroth approximation (0.388, 0.452, and 0.540 for Ti_2C_2, Sc_3N, and Y_3N species, respectively).

Moreover, we have separated different bonds into [6,6] and [5,6] bond types to see if we find different behaviors for these two types of bonds (see Figures 1 and 2). In general, better correlation factors are found for [6,6] bond types (between 0.733 and 0.945) than for [5,6] bond types (between 0.704 and 0.902). The additions to the [5,6] bonds of Sc_3N@D_{3h}-C_{78} represent the only exception to the good correlations found between reaction energies and energy barriers. In this case, ranges observed in reaction energies and barriers are small (from 19.7 to 22.3 kcal mol^{-1} for reaction barriers and from −10.4 to −4.3 kcal mol^{-1} for the reaction energies) and this results in a worse correlation. Even so, as can be seen in Table S1 in the Supporting Information, the two most reactive [5,6] bonds from the kinetic and thermodynamic points of view are coincident. As discussed later, application of the present FCM approach requires only that the kinetic and thermodynamic most reactive bonds match. Also, we can see that [6,6] and [5,6] bond types follow different slopes; [6,6] bonds are those with the slope closest to the expected 1/2 and hence follow the linear Dimroth approximation better. This is in agreement with the fact that the [5,6] bond is, in general, more exothermic than [6,6] ones, with [6,6] additions being closer to thermoneutral.

In a previous study,[33] Osuna and Houk showed that although several cases exist where the BEP relationship (Dimroth approximation) between energy barriers and reaction energies is fulfilled, this approximation *is not a general rule* followed by all cycloaddition reactions. In fact, Slanina et al. found that in the oxygen addition to the [5,6] and [6,6] bonds of C_{60}, the thermodynamic and the kinetic stability order of the two types of bonds are reversed.[34] Nevertheless, our results show that, for EMFs, which have cycloaddition reactions with lower exothermicities than free cages, there is a good correlation between energy barriers and reaction energies. Moreover, we are always comparing cycloaddition reactions taking place on the same species (the same EMF) but over different nonequivalent bonds.

dx.doi.org/10.1021/ct300044x | J. Chem. Theory Comput. 2012, 8, 1671–1683

Therefore, we can conclude that DA cycloadditions on different bonds of the same EMF fulfill the Dimroth approximation. Consequently, in EMF cycloaddition reactions thermodynamic (reaction energies) and kinetic (energy barriers) results produce the same or similar orderings of reactivity. This is an important feature to take into account for the study of regioselectivity of cycloadditions where EMFs are present.

B. Evaluation of the Distortion/Interaction Model for Diels–Alder Cycloadditions Involving Endohedral Metallofullerene Derivatives: Role of the Distortion or Deformation Energies. The distortion or deformation energy of the TS defined first by Morokuma[35] corresponds to the energy required to distort the diene and dienophile to the geometries they have in the TS without allowing interaction between both reactants. Using this definition, one can split the energy barrier into distortion and interaction energies, i.e., $\Delta E^{\ddagger} = \Delta E_d^{\ddagger} + \Delta E_i^{\ddagger}$ (see Figure 5). Deformation energies are always destabilizing, while the interaction term is usually stabilizing. In the present work, we have to keep in mind that we are working with energies obtained with single point calculations (BP86/TZP) using molecular structures optimized at a lower level of theory (BP86/DZP). For this reason, it is possible to obtain slightly negative deformation energies or positive interaction energies as the structures are not true minima at the BP86/TZP level of theory.

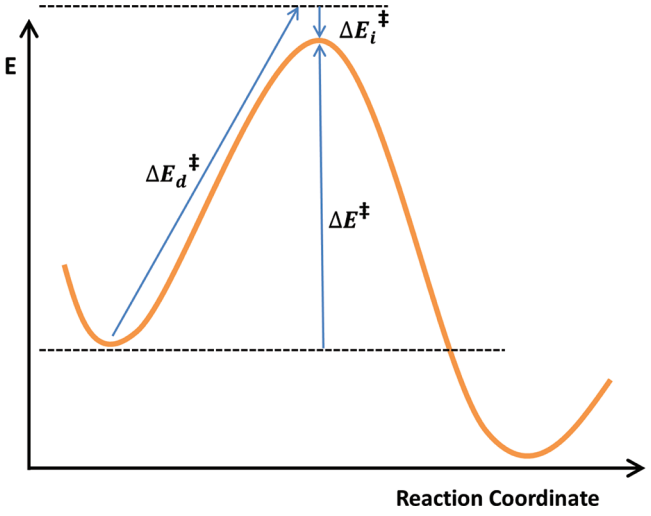

Figure 5. Schematic representation of the activation ($\Delta E^{\ddagger}$), distortion ($\Delta E_d^{\ddagger}$), and interaction ($\Delta E_i^{\ddagger}$) energies.

In 1999, Bickelhaupt[36] proposed to use TS distortion energies to better understand the reactivity of some organic reactions. He called this approach the "activation strain model".[37] Later on, Ess and Houk used this model (named by these authors as the "distortion/interaction model") to provide a new way of understanding the reactivity trends for cycloaddition reactions.[38] They showed that the energy to distort the 1,3-dipole and dipolarophile to the TS geometry controls the kinetics of cycloaddition reactions with alkenes or alkynes, rather than frontier molecular orbital interactions or thermodynamics. In this section, we assess the performance of the activation strain or distortion/interaction model to provide rationalization of the regioselectivity of DA in EMFs.

Table 1 contains the energy barriers and their distortion (for *s-cis*-1,3-butadiene, EMFs, and their sum) and interaction components for the DA cycloaddition reactions between *s-cis*-1,3-butadiene and C_{78} and $Ti_2C_2@C_{78}$ EMF. Here, we will discuss the Ti_2C_2 case, but the arguments are also valid for the Sc_3N and Y_3N EMFs ($Sc_3N@C_{78}$ and $Y_3N@C_{78}$ values are given in Table S2 in the Supporting Information). As can be seen in Table 1, the diene deformation energy is generally larger than the fullerene one. It is usually found that the shorter the C–C distance of the bonds being formed (i.e., the later the TS), the larger the distortion energy of the diene as their CCC angles and CCCH dihedral angles are much distorted with respect to the initial geometry, requiring more energy to achieve the TS geometry.

Figure 6a depicts the energy barriers versus distortion energies (diene, fullerene, and total distortion energies) for the $Y_3N@C_{78}$ EMF (the information related to the other two studied EMFs is depicted in Figure S1 in the Supporting Information). As can be seen, although fullerene and diene distortion energies have good correlations with energy barriers (R^2 is 0.735 and 0.695 for fullerene and diene, respectively), a better correlation factor is obtained when both distortion energies are taken together, that is, when we consider the total distortion energy as the sum of the

Table 1. Energy Barriers ($\Delta E^{\ddagger}$) and Diene, Fullerene, and Total Deformation ($\Delta E_{d,diene}^{\ddagger}$, $\Delta E_{d,ful}^{\ddagger}$, $\Delta E_d^{\ddagger}$) and Interaction ($\Delta E_i^{\ddagger}$) Energies at the Transition State in the Diels–Alder Reaction between *s-cis*-1,3-butadiene and All Nonequivalent Bonds of D_{3h}-C_{78} and $Ti_2C_2@D_{3h}$-C_{78} at the BP86/TZP//BP86/DZP Level[a]

		D_{3h}-C_{78}					$Ti_2C_2@D_{3h}$-C_{78}[c]				
product	bond type	$\Delta E^{\ddagger}$[b]	$\Delta E_{d,ful}^{\ddagger}$	$\Delta E_{d,diene}^{\ddagger}$	$\Delta E_d^{\ddagger}$	$\Delta E_i^{\ddagger}$	$\Delta E^{\ddagger}$	$\Delta E_{d,ful}^{\ddagger}$	$\Delta E_{d,diene}^{\ddagger}$	$\Delta E_d^{\ddagger}$	$\Delta E_i^{\ddagger}$
1	A [6,6]	**12.2**	4.7	13.9	18.5	−6.3	23.6	9.2	17.2	26.3	−2.7
2	C [6,6]	30.2	18.3	27.8	46.0	−15.8	26.8	19.6	24.8	44.4	−17.6
3	B [6,6]	21.7	7.0	9.4	16.4	5.3	**18.2**	8.8	12.6	21.5	−3.2
4	B [6,6]	14.8	6.7	9.3	16.0	−1.2	29.6	20.3	31.2	51.5	−21.9
5	B [6,6]	14.4	6.7	9.1	15.8	−1.4	20.6	10.6	12.1	22.7	−2.1
6	B [6,6]	17.2	8.8	11.1	19.9	−2.7	27.0	23.7	30.5	54.1	−27.1
7	A [6,6]	**13.5**	3.9	12.5	16.4	−2.9	27.5	15.6	19.6	35.3	−7.7
a	D [5,6]	17.2	7.8	11.5	19.2	−2.0	21.4	9.0	16.1	25.1	−3.7
b	D [5,6]	**12.5**	4.7	10.0	14.6	−2.1	26.5	17.8	27.9	45.7	−19.2
c	D [5,6]	16.7	7.8	9.5	17.3	−0.6	**17.4**	7.2	11.6	18.8	−1.4
d	D [5,6]	22.1	16.2	22.8	39.0	−16.9	22.6	11.8	15.1	26.9	−4.4
e	D [5,6]	15.3	6.6	9.6	16.1	−0.8	20.5	12.7	10.1	22.9	−2.3
f	D [5,6]	18.0	8.3	10.0	18.4	−0.4	**19.3**	12.2	9.1	21.3	−2.0

[a]Bold values indicate the bonds that are the most reactive under kinetic control. All energies are given in kcal·mol^{-1}. [b]Values from ref 11. [c]Values from ref 13.

dx.doi.org/10.1021/ct300044x | J. Chem. Theory Comput. 2012, 8, 1671–1683

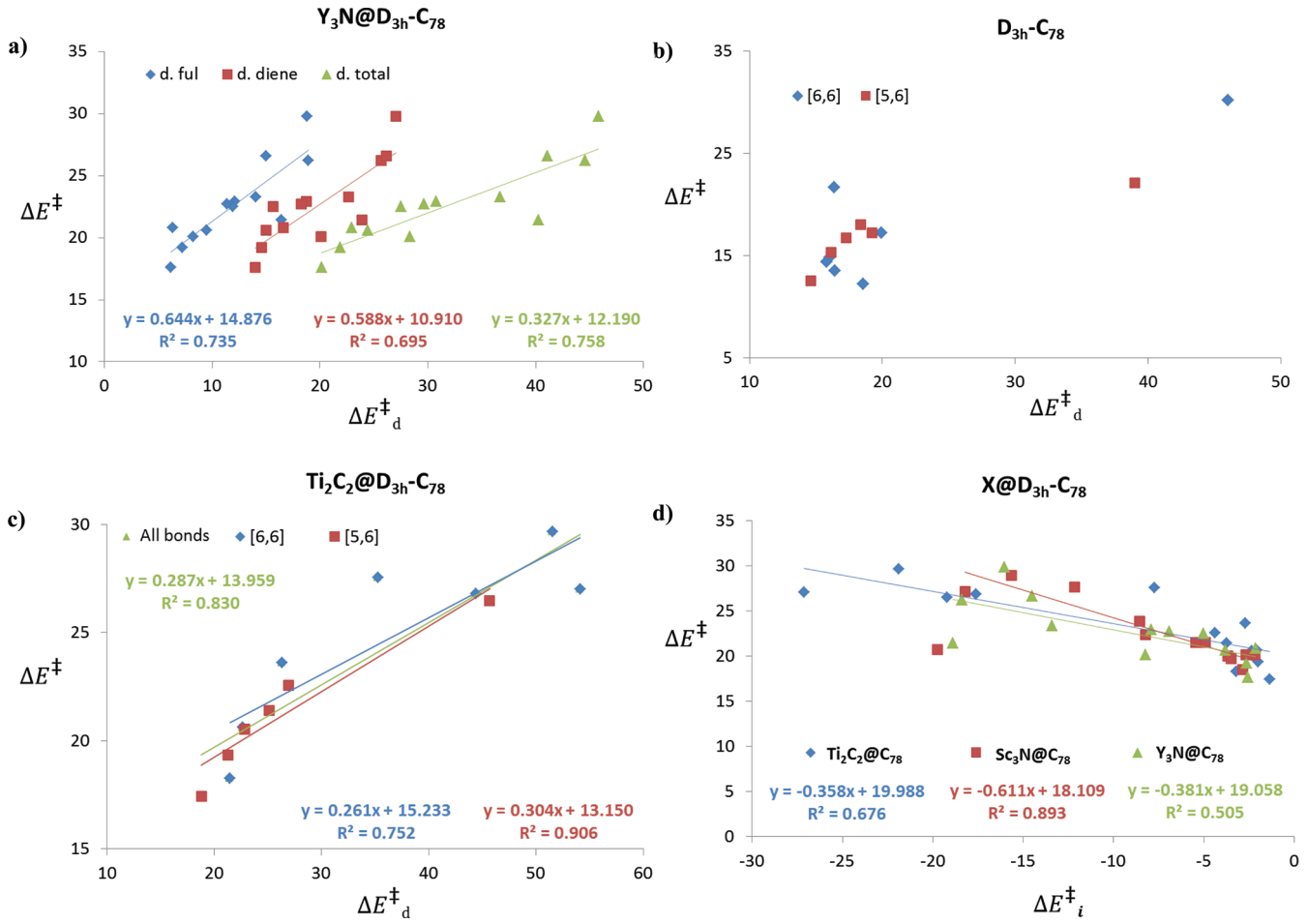

Figure 6. Plot of BP86/TZP//BP86/DZP reaction barriers ($\Delta E^{\ddagger}$) versus (a) fullerene (blue), diene (red), and total (green) distortion energies ($\Delta E^{\ddagger}_{d,ful}$, $\Delta E^{\ddagger}_{d,diene}$, and $\Delta E^{\ddagger}_{d}$) for the Diels–Alder reaction of *s-cis*-1,3-butadiene with $Y_3N@D_{3h}$-C_{78}; (b) [6,6] (blue), and [5,6] (red) bond distortion energies ($\Delta E^{\ddagger}_{d,[6,6]}$ and $\Delta E^{\ddagger}_{d,[5,6]}$) for the Diels–Alder reaction of *s-cis*-1,3-butadiene with free D_{3h}-C_{78}; (c) total (green), [6,6] (blue), and [5,6] (red) bond distortion energies ($\Delta E^{\ddagger}_{d}$, $\Delta E^{\ddagger}_{d,[6,6]}$, and $\Delta E^{\ddagger}_{d,[5,6]}$) for the Diels–Alder reaction of *s-cis*-1,3-butadiene with $Ti_2C_2@D_{3h}$-C_{78}; and (d) interaction energies ($\Delta E^{\ddagger}_{i}$) for the Diels–Alder reaction of *s-cis*-1,3-butadiene with $X@D_{3h}$-C_{78} (X = Ti_2C_2 (blue), Sc_3N (red), and Y_3N (green)). Energies in kcal·mol^{-1}.

fullerene and diene distortion energies (in the $Y_3N@C_{78}$ system, R^2 for the total distortion energy is 0.758). On the other hand, parts b and c of Figure 6 show the representation of energy barriers ($\Delta E^{\ddagger}$) versus the total distortion energies ($\Delta E^{\ddagger}_{d}$) found for all DA cycloadditions over all nonequivalent bonds in free C_{78} and $Ti_2C_2@C_{78}$ systems, respectively ($Sc_3N@C_{78}$ and $Y_3N@C_{78}$ plots are given in Figure S2 in the Supporting Information). We have also separated the energy barriers between those corresponding to the [6,6] and [5,6] bond types. Although good correlations between energy barriers and total distortion energies are found for EMFs, as indicated by the R^2 values obtained (0.830, 0.745, and 0.758 for $Ti_2C_2@C_{78}$, $Sc_3N@C_{78}$, and $Y_3N@C_{78}$, respectively), no correlation exists at all for the free C_{78} fullerene case. This is likely the result of energy barriers in free C_{78} fullerene being more scattered over a larger range (12.2–30.2 kcal mol^{-1}) than in EMFs. The bonds of EMFs that are more similar in reactivity seem to favor better correlations. By comparing the two bond types, [6,6] and [5,6], we can observe parallel behaviors. Both types show a good correlation between energy barriers and total distortion energies, and no significant differences are found.

Interaction energy terms are always negative (with the only exception of bond 3 for free C_{78}), but they are small in absolute value compared with total distortion energies. As has been reported,[33] the larger contribution to the energy barrier for these cycloaddition reactions involving fullerene species comes from the energy requirements to distort both reactants instead of the interaction energy between them. To analyze the interaction energies, we have represented in Figure 6d the energy barriers ($\Delta E^{\ddagger}$) versus the interaction energies ($\Delta E_i^{\ddagger}$) found for Ti_2C_2, Sc_3N, and Y_3N EMFs. As can be seen, reasonable linear correlations are found in all cases. It is clearly seen in Figure 6d that the most reactive bonds usually have the smallest (in absolute value) interaction energies.

The distortion/interaction model is a powerful tool for understanding and interpreting the different reactivities of all nonequivalent bonds present in an EMF, especially when frontier molecular orbital analysis gives poor results. However, since we need the TS geometry for applying it, the model cannot be used to reduce the high computational cost of regioselectivity studies in EMFs. This is in particular true since any candidate for TS has to be validated through the costly frequency analysis to have one (*and only one*) imaginary frequency.

C. Noncluster Model as a Tool for the Analysis of Endohedral Metallofullerene Exohedral Reactivity: Metallic Cluster Effects on Transition State and Product Structures. In a recent study,[13] we have introduced a new

Table 2. Energy Barriers ($\Delta E^{\ddagger}$), Noncluster Energy Barriers ($\Delta E^{\ddagger}_{NC}$), Increment of Noncluster Energy Barriers ($\Delta\Delta E^{\ddagger}_{NC}$), and Noncluster Energy Barriers with Six Electrons Added ($\Delta E^{\ddagger}_{NC+6e^-}$) for All Nonequivalent Bonds Being Formed at the TS in the Diels–Alder Reaction between *s-cis*-1,3-butadiene and X@D_{3h}-C_{78} (X = Ti_2C_2, Sc_3N, Y_3N) at the BP86/TZP//BP86/DZP Level[a]

		D_{3h}-C_{78}	$Ti_2C_2@D_{3h}$-C_{78}				$Sc_3N@D_{3h}$-C_{78}				$Y_3N@D_{3h}$-C_{78}			
product	bond type	$\Delta E^{\ddagger}$ [b]	$\Delta E^{\ddagger}$ [c]	$\Delta E^{\ddagger}_{NC}$ [c]	$\Delta\Delta E^{\ddagger}_{NC}$ [c]	$\Delta E^{\ddagger}_{NC+6e^-}$	$\Delta E^{\ddagger}$ [b]	$\Delta E^{\ddagger}_{NC}$	$\Delta\Delta E^{\ddagger}_{NC}$	$\Delta E^{\ddagger}_{NC+6e^-}$	$\Delta E^{\ddagger}$ [b]	$\Delta E^{\ddagger}_{NC}$	$\Delta\Delta E^{\ddagger}_{NC}$	$\Delta E^{\ddagger}_{NC+6e^-}$
1	A [6,6]	**12.2**	23.6	6.8	16.7	4.8	23.8	4.3	19.5	−1.1	20.1	5.1	15.0	−5.3
2	C [6,6]	30.2	26.8	25.6	1.2	3.3	27.1	30.4	−3.3	9.1	26.2	36.5	−10.3	10.2
3	B [6,6]	21.7	**18.2**	17.4	0.9	4.8	28.9	33.7	−4.8	8.3	26.6	26.8	−0.2	−0.6
4	B [6,6]	14.8	29.6	6.8	22.9	−5.1	20.0	20.4	−0.4	9.4	20.6	35.8	−15.2	9.5
5	B [6,6]	14.4	20.6	8.1	12.5	−14.9	27.6	25.5	2.1	15.7	29.8	40.1	−10.3	17.7
6	B [6,6]	17.2	27.0	21.5	5.6	−3.7	**18.5**	22.6	−4.1	4.0	**19.2**	33.3	−14.1	−0.5
7	A [6,6]	**13.5**	27.5	3.5	24.0	−4.1	20.1	16.8	3.3	8.3	20.8	12.6	8.2	7.6
a	D [5,6]	17.2	21.4	11.0	10.4	−2.8	21.5	14.6	6.9	−10.4	22.9	12.6	10.3	−9.6
b	D [5,6]	**12.5**	26.5	−1.2	27.7	−9.1	20.7	8.5	12.2	−5.9	21.4	4.1	17.3	−4.6
c	D [5,6]	16.7	**17.4**	14.1	3.4	−7.3	20.1	14.5	5.6	−7.0	22.5	8.8	13.7	−9.4
d	D [5,6]	22.1	22.6	11.7	10.9	−11.6	**19.7**	16.7	3.0	−8.4	**17.6**	12.8	4.8	−9.6
e	D [5,6]	15.3	20.5	7.7	12.9	−17.7	22.3	11.9	10.4	−10.9	23.3	22.2	1.1	−7.8
f	D [5,6]	18.0	**19.3**	25.2	−5.8	−14.6	21.5	16.1	5.4	−14.3	22.7	19.4	3.3	−8.4
	all bonds	17.4	22.9	11.8	11.1	−7.6	22.6	18.8	3.8	−0.4	22.9	22.0	0.9	−0.6
average	[6,6]	17.8	24.2	12.5	11.8	−3.4	24.3	24.3	0.0	9.2	24.2	30.6	−6.3	7.1
	[5,6]	17.0	21.7	11.2	10.5	−11.6	21.0	13.5	7.5	−9.6	21.5	13.8	7.7	−8.0

[a]For comparison, $\Delta E^{\ddagger}$ values of free D_{3h}-C_{78} are also given. Bold values indicate the most reactive bonds under kinetic control. Average values are calculated taking into account the total number of bonds present in the entire fullerene structure. All energies are given in kcal·mol^{-1}. [b]Values from ref 12. Only results for the *up* region of $Y_3N@D_{3h}$-C_{78} are reported here. [c]Values from ref 13.

concept for the analysis of the exohedral reactivity of EMFs, the noncluster (NC) energy barriers ($\Delta E^{\ddagger}_{NC}$). This energy parameter is defined as the energy difference between the TS and reactants when the metallic cluster is removed from the EMF while keeping the geometry of the reactants and TS frozen. Moreover, here we present another related concept, the noncluster distortion energy ($\Delta E^{\ddagger}_{d,NC}$). This new descriptor is defined as the energy required to distort the EMF cage from its optimized geometry in the EMF reactants to the geometry it has in the EMF TS but removing the inner metallic cluster. Thus, it is equivalent to the distortion energy evaluated in subsection B, but without the presence of the metallic cluster. Similarly, in this work we propose to apply the NC model to the product structures to obtain noncluster reaction energies ($\Delta E_{R,NC}$).

The noncluster energy barrier gives an idea of the geometric effect of the cluster on the energy barrier, as only geometric changes in the cage structure are taken into account. However, if we take the difference between the actual energy barrier and the noncluster energy barrier, we get an indication of the electronic effect of the metallic cluster on the energy barrier. We refer to this difference as the increment of noncluster (INC) energy barrier ($\Delta\Delta E^{\ddagger}_{NC}$). If for a given bond $\Delta\Delta E^{\ddagger}_{NC}$ is negative, it implies that the formal charge transfer from the metallic cluster to the fullerene cage favors this addition, and vice versa. When we have small energy differences, it means that charge transfer from the metallic cluster does not have a large effect on the final reactivity of the considered bond. Therefore, the difference between the energy barrier and the noncluster energy barrier is a descriptor of the electronic effect due to the presence of the metallic cluster. This notwithstanding, we have to bear in mind that geometric changes in the fullerene cage when a metallic cluster is encapsulated are at least in part due to electronic effects. Therefore, it is not possible to quantitatively separate in an exact form the electronic and geometric effects due to the presence of the metallic cluster.

With the same line of reasoning, one could think in a possible intermediate step between the NC energy barrier and the final energy barrier that consists in adding to the NC cage the electrons transferred by the metallic cluster. Considering the ionic model proposed for describing EMFs,[39] we have explicitly added six electrons to reactants, TSs, and products of the noncluster structures and we have obtained the noncluster energy barrier/reaction energy with six electrons (NC + $6e^-$ energy barriers, $\Delta E^{\ddagger}_{NC+6e^-}$, and NC + $6e^-$ reaction energy, $\Delta E_{R,NC+6e^-}$). One could expect that in $\Delta E^{\ddagger}_{NC+6e^-}$ and $\Delta E_{R,NC+6e^-}$ the effects of occupying the lowest unoccupied molecular orbitals (LUMOs) of the free cage are already included. Therefore, we have, first, the $\Delta E^{\ddagger}_{NC}$ and $\Delta E_{R,NC}$ that take into account only the geometric effect of the cluster, second, the $\Delta E^{\ddagger}_{NC+6e^-}$ and $\Delta E_{R,NC+6e^-}$ that include the geometric effect and an estimation of the electronic effect, and, finally the actual $\Delta E^{\ddagger}$ and ΔE_R that gather the two joint effects.

C.i. Noncluster Model Applied to Transition State Structures. The results, presented in Table 2, show that no correlation exists between the noncluster energy barrier values and energy barriers for the present EMFs studied (see also the plot representation in Figure S3 in the Supporting Information). Neither is there any correlation between the INC energy barriers and energy barriers in any of the present studied systems. Although, as previously shown,[13] the position and orientation of the metallic cluster versus the considered bond have important consequences for the regioselectivity, the present results indicate that electronic effects induced by the metallic cluster on the energy barriers are not minor.

The comparison of the NC + $6e^-$ energy barrier correlations with respect to the actual energy barriers with the noncluster energy barriers shows that the former do not clearly improve the latter ($\Delta E^{\ddagger}_{NC+6e^-}$ vs $\Delta E^{\ddagger}$, see Table 2 and Figure S3 in the Supporting Information). The lack of correlation comes from the fact that six electrons are added without correctly describing the changes in the LUMO shapes and energies due to the presence of the metallic cluster. Apart from that, the computed

Voronoi charges of the metal cluster inside the fullerene cavity indicate a smaller charge transfer from the metal to the fullerene cage.[13] In our previous work,[13] we have seen that depending on the nature and orientation of the metallic cluster inside the fullerene cage the final shapes and energies of the LUMO orbitals change substantially. This factor is not taken into account by the $\Delta E^{\ddagger}_{NC+6e^-}$ descriptor. In all cases the barriers decrease because the reactants become more destabilized than the TS. We must note that [5,6] bonds are on average more favored by the formal charge transfer than [6,6] bonds. This observation concurs with the fact that charge transferred from the metallic cluster to the fullerene cage is localized mainly on the five-membered rings (5-MRs)[13,40] and also with the fact that [6,6] bonds are less reactive than [5,6] bonds in X@C_{78} (X = Ti_2C_2, Sc_3N, Y_3N) EMFs.[13]

Focusing now our attention on the NC distortion energy ($\Delta E^{\ddagger}_{d,NC}$, including the diene distortion energy), we see that a correlation exists between $\Delta E^{\ddagger}$ and $\Delta E^{\ddagger}_{d,NC}$ (see Figure 7).

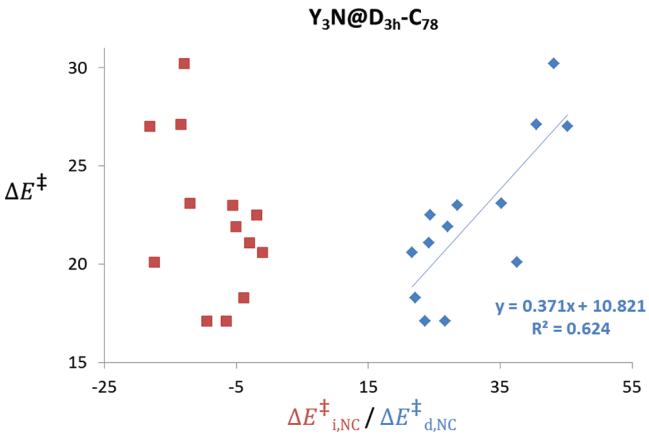

Figure 7. Plot of BP86/TZP//BP86/DZP energy barriers ($\Delta E^{\ddagger}$) versus noncluster total distortion (blue) energies ($\Delta E^{\ddagger}_{d,NC}$) and noncluster interaction (red) energies ($\Delta E^{\ddagger}_{i,NC}$) for the Diels–Alder reaction of *s-cis*-1,3-butadiene with $Y_3N@D_{3h}$-C_{78}. Energies in kcal·mol^{-1}.

Although correlation factors are always lower than 0.9 (plot representations referring to Sc_3N and Ti_2C_2 systems can be found in Figure S4 in the Supporting Information), the most significant fact is that although the metallic cluster from the TS structure has been removed, the correlation found in subsection B is still valid. The interaction energy term calculated as $\Delta E^{\ddagger}_{i,NC} = \Delta E^{\ddagger}_{NC} - \Delta E^{\ddagger}_{d,NC}$ is also represented for $Y_3N@D_{3h}$-C_{78} in Figure 7 (interaction energy values and NC distortion energies are listed in Table S3 in the Supporting Information for all systems studied). As can be seen, there is no correlation between $\Delta E^{\ddagger}_{i,NC}$ and energy barriers. Since we have found that there exists a quite good correlation between reaction barriers and NC distortion energies, the interaction term is responsible for the lack of correlation between $\Delta E^{\ddagger}_{NC}$ and $\Delta E^{\ddagger}$. All these observations give us useful information: although the explicit presence of the metallic cluster inside the fullerene is not necessary to reproduce the distortion energies at the TS structure, it is essential to provide a correct estimate of the interaction energy term.

C.ii. Noncluster Model Applied to Product Structures. In this subsection, we apply the NC model to the product structures to get the NC reaction energies, $\Delta E_{R,NC}$. The procedure to obtain these energy values is equivalent to that followed in the TS case: we perform single point energy calculations of reactants and products after removing the metallic cluster from the reactant and the product EMF structures while keeping the molecular structure of the fullerene frozen. Again, we have evaluated the effect of the explicit inclusion of the six electrons transferred from the metallic cluster to the fullerene structure, obtaining the NC reaction energies with six electrons (NC + 6e$^-$ reaction energies, $\Delta E_{R,NC+6e^-}$).

The $\Delta E_{R,NC}$, $\Delta\Delta E_{R,NC}$, and $\Delta E_{R,NC+6e^-}$ reaction energies for all EMF studied systems (X@D_{3h}-C_{78}, where X = Ti_2C_2, Sc_3N, or Y_3N) are given in Table 3. Again we find that there is not a direct relationship between the reaction energies of the different nonequivalent bonds and the NC ones. Therefore, the presence of the metallic cluster is critical to correctly reproduce the thermodynamics (and kinetics) of the DA cycloaddition reactions involving EMFs.

An important observation is the good correlation we find between the $\Delta E_{R,NC}$ of EMF species and the ΔE_R of the free C_{78} cage. As can be seen in Figure 8, correlation factors R^2 are close to 0.9 (R^2 is 0.767, 0.860, and 0.821 for Ti_2C_2, Sc_3N, and Y_3N EMFs, respectively) which are in general improved when bonds are divided into [6,6] and [5,6] bond types. These surprising results show that although the fullerene structure is distorted in the NC structures, the ordering of reactivity given by the thermodynamics of the DA cycloaddition reaction agrees with that found for the free D_{3h}-C_{78} fullerene when the metallic cluster is removed and the rest of structure is kept frozen. This means that, first, an approximate estimate of the distortion and strain of the fullerene cage is enough for the final determination of the most/least stable products, and, second, that full electronic effects (not a simple six electron transfer) of the cluster are essential to correctly reproduce the ΔE_R values of the EMFs.

D. New Tool for Predicting the Exohedral Diels–Alder Regioselectivity of Endohedral Metallofullerene Derivatives: The Frozen Cage Model. In previous subsections, we have applied different tools to understand the changes in the regioselectivity of the DA cycloadditions to EMFs due to metal cluster encapsulation. First of all, we have seen that there is a good correspondence between thermodynamic and kinetic results for EMF species. In a second step, we have shown that the activation strain or distortion/interaction model is a useful interpretative tool of analysis. Finally, we have seen that the NC reaction energies of EMFs have a good correlation with the reaction energies of the free cage, showing that deformation of the fullerene cage is not as important for the final determination of the most reactive bond in EMFs as the explicit inclusion of the metal cluster.

The good correlation between $\Delta E_{R,NC}$ of EMF species and the ΔE_R of the free C_{78} cage made us wonder whether a correlation exists between the ΔE_R of EMF species and the ΔE_R estimated from single point energy calculations at the frozen free C_{78} cage adducts that incorporate the metallic cluster inside. As shown in the next paragraphs, we find that such a correlation exists. This result is used to propose a new model called the "frozen cage model (FCM)" to predict at very low computational cost the regioselectivity of DA cycloadditions involving EMF derivatives.

The FCM model starts from the different stationary points optimized for the empty fullerene cage. By using the reactant structure, we introduce the metallic cluster inside and, always keeping the fullerene cage frozen, we reoptimize only the metallic cluster structure, maintaining its correct position and

Table 3. Reaction Energies (ΔE_R), Noncluster Reaction Energies ($\Delta E_{R,NC}$), Increment of Noncluster Reaction Energies ($\Delta\Delta E_{R,NC}$), and Noncluster Reaction Energies with Six Electrons Added ($\Delta E_{R,NC+6e^-}$) for All Nonequivalent Bonds Formed for the Diels–Alder Reaction between *s-cis*-1,3-butadiene and X@D_{3h}-C_{78} (X = Ti_2C_2, Sc_3N, Y_3N) at the BP86/TZP//BP86/DZP Level[a]

		D_{3h}-C_{78}	$Ti_2C_2@D_{3h}$-C_{78}				$Sc_3N@D_{3h}$-C_{78}				$Y_3N@D_{3h}$-C_{78}			
product	bond type	ΔE_R[b]	ΔE_R[c]	$\Delta E_{R,NC}$	$\Delta\Delta E_{R,NC}$	$\Delta E_{R,NC+6e^-}$	ΔE_R[b]	$\Delta E_{R,NC}$	$\Delta\Delta E_{R,NC}$	$\Delta E_{R,NC+6e^-}$	ΔE_R[b]	$\Delta E_{R,NC}$	$\Delta\Delta E_{R,NC}$	$\Delta E_{R,NC+6e^-}$
1	A [6,6]	**−16.0**	−2.6	−16.6	13.9	−0.5	4.0	−23.6	27.6	0.2	−5.4	−23.6	18.2	−1.1
2	C [6,6]	12.5	4.2	12.7	−8.5	6.8	6.1	13.7	−7.6	9.0	5.8	11.1	−5.3	8.1
3	B [6,6]	1.8	**−14.1**	−4.6	−9.5	−2.2	9.2	12.0	−2.8	−0.8	0.6	−1.3	1.9	−1.6
4	B [6,6]	−9.2	8.5	−13.7	22.3	−0.9	**−9.7**	−8.6	−1.1	0.5	−8.7	−9.9	1.2	−0.4
5	B [6,6]	0.9	1.6	−5.4	7.0	3.4	5.9	−2.3	8.2	6.3	10	3.1	6.9	7.3
6	B [6,6]	4.0	11.1	2.5	8.6	−3.5	**−12.7**	7.3	−20.0	0.4	**−10.6**	12.1	−22.7	0.1
7	A [6,6]	**−18.8**	5.1	−10.4	15.5	−1.0	−7.6	−15.5	7.9	−0.9	−6.6	−18.5	11.9	−1.6
a	D [5,6]	−8.8	−7.1	−19.4	12.2	−11.5	−6.0	−14.3	8.3	−9.5	−3.4	−16.1	12.7	−9.1
b	D [5,6]	**−23.9**	3.4	−34.2	37.6	18.7	−4.3	−28.3	24.0	−3.0	−1.7	−27.7	26.0	−2.8
c	D [5,6]	−13.3	**−18.1**	−21.5	3.4	−13.7	**−10.4**	−21.0	10.6	−11.9	−6.1	−24.2	18.1	−10.9
d	D [5,6]	−5.2	−6.8	−17.6	10.8	−10.1	−7.6	−13.6	6.0	−9.2	**−13.4**	−18.2	4.8	−10.8
e	D [5,6]	−13.8	−5.5	−20.9	15.5	−6.7	−4.9	−18.1	13.2	−4.8	−2.7	−19.1	4.1	−4.3
f	D [5,6]	−5.9	**−14.6**	−16.3	1.7	−9.4	−6.5	−12.0	5.5	−8.3	−5.6	−17.7	12.1	−9.1
	all bonds	−7.3	−3.1	−13.8	10.7	−1.9	−3.3	−9.4	6.1	−2.6	−3.4	−10.5	7.1	−2.9
average	[6,6]	−2.5	1.2	−5.4	6.5	0.3	−0.1	−0.4	0.3	2.2	−1.1	−2.5	1.4	1.8
	[5,6]	−12.0	−7.2	−21.9	14.7	−4.0	−6.3	−17.9	11.6	−7.2	−5.6	−18.1	12.5	−7.4

[a]For comparison, ΔE_R values of free D_{3h}-C_{78} are also given. Bold values indicate the bonds that are the most reactive under thermodynamic control. Average values are calculated taking into account the total number of bonds present in the entire fullerene structure. All energies are given in kcal·mol^{-1}. [b]Values from ref 12. Only results for the *up* region of $Y_3N@D_{3h}$-C_{78} are reported here. [c]Values from ref 13.

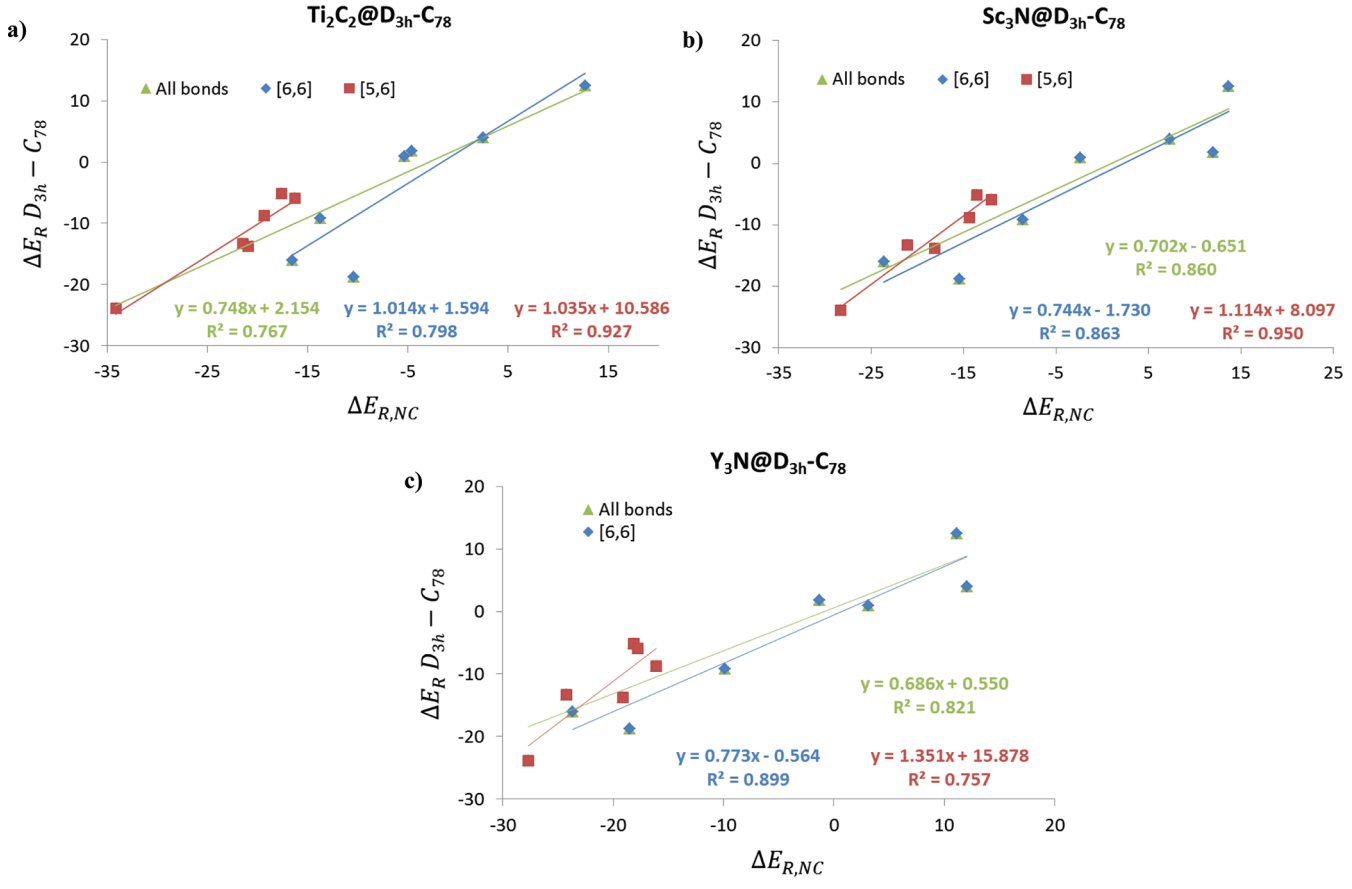

Figure 8. Plot of BP86/TZP//BP86/DZP reaction energies of free D_{3h}-C_{78} fullerene (ΔE_R) versus noncluster reaction energy ($\Delta E_{R,NC}$) for the Diels–Alder reaction of *s-cis*-1,3-butadiene (green) with X@D_{3h}-C_{78}, where X = (a) Ti_2C_2, (b) Sc_3N, and (c) Y_3N. We have also represented the two different bond types [6,6] (blue) and [5,6] (red). Energies in kcal·mol^{-1}.

orientation inside the cage. That is, we center the metal cluster inside the cage and align it with the corresponding axis and/or symmetry planes (in D_{3h}-C_{78} cage, with the C_3 symmetry axis and horizontal and vertical symmetry planes; see for example

dx.doi.org/10.1021/ct300044x | J. Chem. Theory Comput. 2012, 8, 1671–1683

Table 4. Reaction Energies (ΔE_R), Frozen Cage Model Reaction Energies ($\Delta E_{R,FCM}$), and Absolute Errors ($A_{error} = |\Delta E_R - \Delta E_{R,FCM}|$) for Diels–Alder Reactions between *s-cis*-1,3-butadiene and All Nonequivalent Bonds of X@D_{3h}-C_{78} (X = Ti_2C_2, Sc_3N, Y_3N) at the BP86/TZP//BP86/DZP Level[a]

		$Ti_2C_2@D_{3h}$-C_{78}			$Sc_3N@D_{3h}$-C_{78}			$Y_3N@D_{3h}$-C_{78}		
product	bond type	ΔE_R[b]	$\Delta E_{R,FCM}$	A_{error}	ΔE_R[c]	$\Delta E_{R,FCM}$	A_{error}	ΔE_R[c]	$\Delta E_{R,FCM}$	A_{error}
1	A [6,6]	**−2.6**	**−4.3**	1.7	4.0	−2.8	6.8	−5.4	−3.5	1.9
2	C [6,6]	4.2	8.9	4.7	6.1	8.4	2.3	5.8	3.2	2.6
3	B [6,6]	**−14.1**	**−14.2**	0.1	9.2	7.0	2.2	0.6	5.5	4.9
4	B [6,6]	8.5	9.6	1.1	**−9.7**	**−8.3**	1.4	**−8.7**	**−10.3**	1.6
5	B [6,6]	1.6	−1.0	2.6	5.9	6.7	0.8	10	7.7	2.3
6	B [6,6]	11.1	9.8	1.3	**−12.7**	**−5.5**	7.2	**−10.6**	**−6.2**	4.4
7	A [6,6]	5.1	3.1	1.9	**−7.6**	**−7.0**	0.6	**−6.6**	**−7.5**	0.9
a	D [5,6]	**−7.1**	**−6.6**	0.5	−6.0	−7.1	1.1	−3.4	−3.9	0.5
b	D [5,6]	3.4	−4.9	8.3	−4.3	−3.6	0.7	−1.7	−5.8	4.1
c	D [5,6]	**−18.1**	**−23.1**	5.0	**−10.4**	**−15.0**	4.6	**−6.1**	**−13.5**	7.4
d	D [5,6]	−6.8	−11.3	4.5	**−7.6**	**−16.1**	8.5	**−13.4**	**−19.5**	6.1
e	D [5,6]	−5.5	−4.9	0.6	−4.9	−7.1	2.2	−2.7	−10.5	7.8
f	D [5,6]	**−14.6**	**−12.7**	2.0	**−6.5**	**−11.5**	5.0	**−5.6**	**−14.6**	9.0
	all bonds	−3.1	−4.6	2.7	−3.3	−4.8	3.1	−3.4	−6.4	4.5
average	[6,6]	1.2	0.9	1.7	−0.1	0.6	2.4	−1.1	−0.7	2.8
	[5,6]	−7.2	−9.7	3.6	−6.3	−9.9	3.9	−5.6	−11.8	6.2

[a]Bold values indicate the most reactive bonds under thermodynamic control, discriminating by bond type ([6,6] and [5,6]). Average values are calculated taking into account the total number of bonds present in the entire fullerene structure. All energies are given in kcal·mol^{-1}. [b]Values from ref 13. [c]Values from ref 12. Only results for the *up* region of $Y_3N@D_{3h}$-C_{78} are reported here.

Figure 2). The reoptimization is needed because sometimes the size and the shape of the metallic cluster do not allow for an easy inclusion inside the frozen free fullerene cage, as, e.g., the case $Y_3N@C_{78}$.[12] Moreover, in some cages the cluster is deformed. Once we have the correct new geometry of the metallic cluster, then we can add it inside the different product structures optimized for the free fullerene, while keeping the orientation and position of the cluster as found in the reactants. Subsequently, we perform single point energy calculations for each FCM structure and in that way we obtain the FCM reaction energies ($\Delta E_{R,FCM}$) and energy barriers ($\Delta E^{\ddagger}_{FCM}$).

Table 4 gathers the values of the FCM reaction energies ($\Delta E_{R,FCM}$) compared with the respective reaction energies (ΔE_R computed at the BP86/TZP//BP86/DZP level) found for each cycloaddition over all nonequivalent bonds of the Ti_2C_2, Sc_3N, and Y_3N EMFs of the D_{3h}-C_{78} fullerene. Although the values of both energy parameters are different, the errors are small (the average values of absolute errors are 2.7, 3.1, and 4.5 kcal·mol^{-1} for Ti_2C_2, Sc_3N, and Y_3N, respectively), showing that FCM reaction energies reproduce quite well the actual reaction energies of these cycloaddition reactions. The larger errors are always found for [5,6] bond types. This observation reveals two different behaviors in the series, one for each bond type. In Figure 9 we have plotted reaction energies versus FCM reaction energies for the three studied systems and we have represented the two bond types [6,6] and [5,6] in different series. There exist good correlations for all cases, although correlation factors are lower than 0.9. In general, [6,6] bond types have much better R^2 factors (in Ti_2C_2 and Y_3N systems R^2 is 0.921 and 0.833, respectively) than [5,6] ones (between 0.7 and 0.8 for the three cases). Different slopes are found for the two bond types, the [6,6] being closer to 1.0 than the [5,6] slopes that are always lower (with the only exception of Ti_2C_2 EMF; see Figure 9).

Having two distinct trends, one for [6,6] and the other for [5,6] bond types, it seems better to treat the two types separately. In that sense, Table 4 lists in bold the most favored additions under thermodynamic control (more negative reaction energies) and the most favored ones from the FCM point of view for each type of bond. We find that the three most reactive bonds of each bond type ([5,6] and [6,6]) under thermodynamic control always match those most reactive in the FCM. This means that the FCM model can predict which bonds are the most reactive in the EMF derivative under thermodynamic control with simple single point energy calculations. In addition, we have also tested the performance of the FCM for predicting reaction energies when using smaller basis sets such as the double- and single-ζ basis sets. The results obtained (reported in Table S4 and Figure S5 in the Supporting Information) still correctly reproduce the order of the most reactive bonds. Therefore, for a first estimate of the thermodynamic regioselectivity of the DA cycloaddition reaction, these smaller basis sets could also be used to further reduce the computational cost.

In subsection C.ii we have shown that one can reproduce the reaction energies of the free fullerene cage with the NC EMF product structures. Now, we have found that the reaction energies of the EMFs can be estimated from the empty fullerene optimized structures of reactants and products by introducing the metallic cluster a posteriori. In both cases, we have used the same conditions, as we have not reoptimized the model structures. Therefore, FCM is accomplished because the relative stabilities of the different products with respect to reactants do not have large fullerene deformation dependence, as we have seen in subsection C.ii with the NC model.

In the next step, we have investigated the application of the FCM to estimate actual $\Delta E^{\ddagger}$ in EMFs from the calculation of $\Delta E^{\ddagger}_{FCM}$. Results obtained are not as good as thermodynamic ones are, and the reason is easy to understand. In the FCM approximation we are using the TS structures optimized for the free C_{78} species. As reported in previous works,[11−13] differences in the C−C bonds being formed on the TS structures are quite

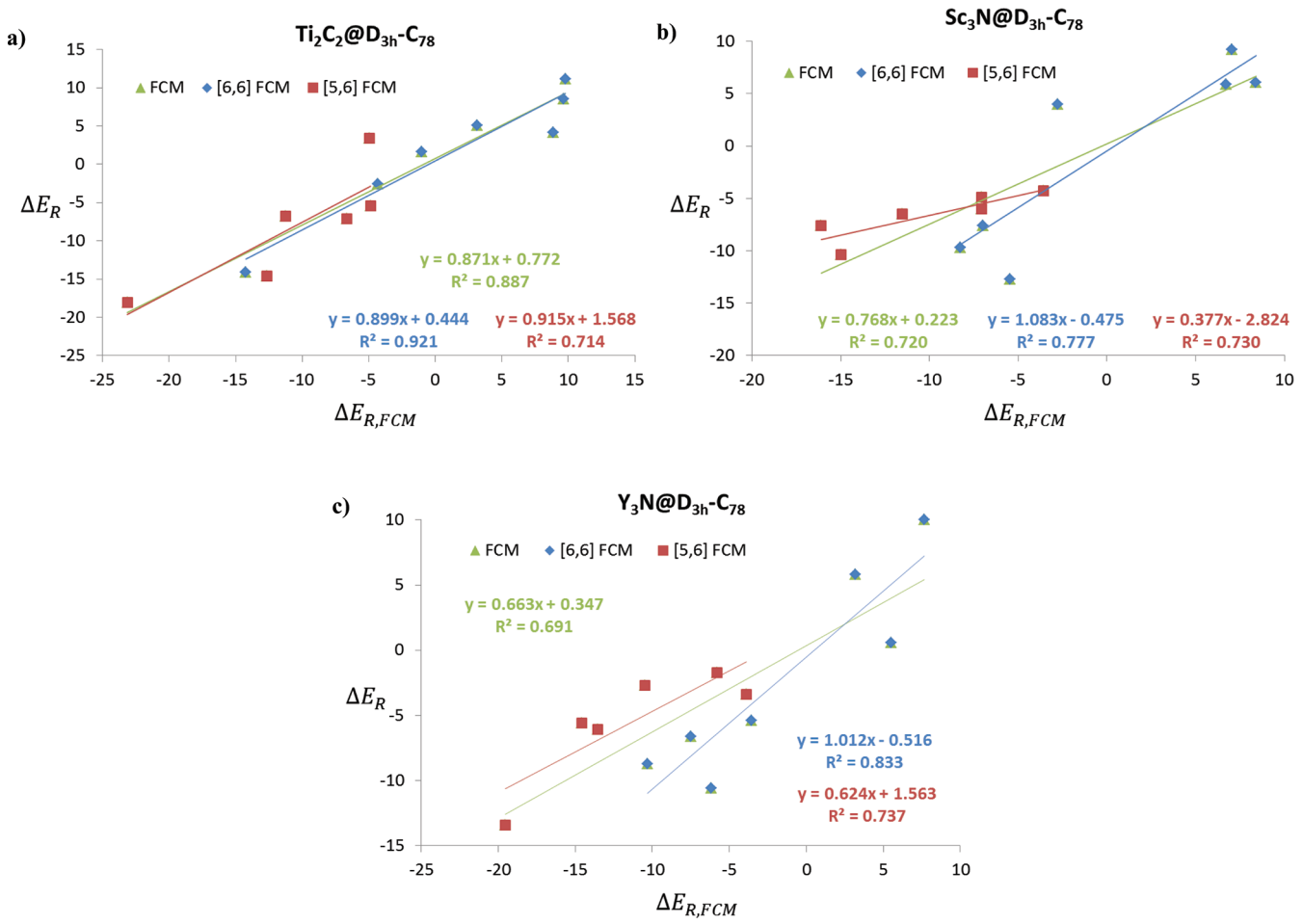

Figure 9. Plot of BP86/TZP//BP86/DZP reaction energies of X@D_{3h}-C_{78} EMFs (ΔE_R) versus frozen cage model reaction energy ($\Delta E_{R,FCM}$) for the Diels–Alder reaction of *s-cis*-1,3-butadiene (green) with X@D_{3h}-C_{78} where X = (a) Ti_2C_2, (b) Sc_3N, and (c) Y_3N. We have also represented the two different bond types [6,6] (blue) and [5,6] (red). Energies in kcal·mol^{-1}.

large when going from free fullerene to the EMFs. These structural differences induce dramatic changes on the orbital overlaps between two interacting molecules that affect directly the energy obtained, making the FCM not valid for the TS structure treatment. The most important error in the $\Delta E^{\ddagger}_{FCM}$ comes from the estimation of the interaction term. This is not surprising if we take into account the results of previous subsections showing that the interaction term in the activation strain or interaction/distortion model is the one which is more metallic cluster dependent (its presence is essential to correctly describe this term). Apart from that, structural differences between free fullerene and EMFs are not so important in the products and this explains why the FCM model is successful for the prediction of the thermodynamics but not for the kinetics.

We have now discussed why FCM works well for reaction energies and not for energy barrier estimations. FCM is, therefore, a good predictive tool of the thermodynamics. However, as we have shown in subsection A, for EMFs kinetic and thermodynamic products are related by the linear Dimroth approximation. As explained before, this means that thermodynamically most favored products match with the kinetic ones. Thanks to this linear relationship, our FCM, although not correctly describing the energy barriers, can be used to predict the kinetically most reactive cycloadditions on EMFs from the thermodynamic results. Within the proposed model, there is no need to perform the computationally expensive TS searches, as FCM only requires the optimized product structures.

Once we have shown the performance of the FCM method, our recommendation in studies of EMF regioselectivity is to use the FCM approach to select the three most reactive bonds of each type ([5,6] and [6,6]) and then to perform a full thermodynamic and kinetic study ascribed only to the selected bonds. In this way one can expect to have very large CPU time savings.

The reason for the absolute errors ($A_{error} = |\Delta E_R - \Delta E_{R,FCM}|$) listed in Table 4 has to be attributed to the lack of geometry reoptimization after metallic cluster encapsulation that will result in bond length alterations and changes in pyramidalization angles. It seems reasonable to think that one could partially include this effect by adding to the correlation the changes in the bond lengths and in pyramidalization angles between EMFs and empty fullerene reactant structures in order to see if the correlation is improved. To test this hypothesis, we have carried out multiple linear regressions such as $\Delta E_R = a\Delta E_{R,FCM} + b\Delta R + c\Delta\theta$ (where ΔR is the increment of the bond lengths (angstroms) and $\Delta\theta$ is the increment of the pyramidalization angles (degrees) when going from free to EMF reactant, and a, b, and c are the parameters adjusted for each multiple regression). The R^2 and p values obtained for all multilinear regressions are gathered in Tables S5a and S5b in the Supporting Information. Focusing on the evolution of the p values when we add more variables into the

dx.doi.org/10.1021/ct300044x | J. Chem. Theory Comput. 2012, 8, 1671–1683

fitting, we can see that the correlations are in general not improved. Only [6,6] and [5,6] bond type series for Sc_3N EMF and [5,6] for Y_3N EMF are improved, but there does not exist a clear-cut behavior. That means that, in general, these two geometric parameters do not increase the predictive value of the FCM.

Results obtained from the multilinear regression studies show us that, although in some cases the inclusion of the proposed geometric parameters improves the correlations found, this is not a general rule. Therefore, in order to improve the FCM estimation of reaction energies, other ways to include the missing geometric information have to be investigated. Even though FCM reaction energies are not accurate enough for quantitative purposes, from a qualitative point of view the predictive power is excellent. In this sense, we believe that the FCM model proposed here will become a very computationally efficient tool to study the regioselectivity of cycloaddition reactions involving EMF derivatives.

CONCLUDING REMARKS

In the present study, we have analyzed the Diels−Alder cycloadditions of *s-cis*-1,3-butadiene to all nonequivalent bonds of X@D_{3h}-C_{78} (X = Ti_2C_2, Sc_3N, and Y_3N) EMFs and we have reached the following conclusions:

1. The linear Dimroth approximation that relates the reaction energies and energy barriers is obeyed.
2. Application of the activation strain or distortion/interaction model indicates a good correlation between energy barriers and distortion energies, but not with interaction energies.
3. Neither noncluster energy barriers nor noncluster distortion energies or increment of noncluster energy barriers correlate with EMF energy barriers. Addition of six electrons to the noncluster model does not improve correlations either. These results indicate that the presence of the metal cluster is fundamental to correctly describing the shape and energy of LUMO orbitals of the cage involved in the interaction with the highest occupied molecular orbital of the diene.
4. There is no direct relationship between EMF reaction energies and the related noncluster reaction energies.
5. There is a good correspondence between EMF noncluster reaction energies and the reaction energies of the free cage.

The information listed above leads us to suggest a fast and computationally low-cost method, the frozen cage model (FCM), to perform accurate qualitative predictions of the exohedral regioselectivity of cycloaddition reactions in EMFs. This FCM approach, which requires only single point energy calculations at the optimized geometries of the free fullerene products, can be used to make a selection of the most reactive bonds in EMFs. This selection process is computationally extremely cheap. Once these bonds are chosen, a full thermodynamic and kinetic study ascribed only to the selected bonds allows obtaining an accurate description of the regioselectivity of the cycloaddition studied with very large CPU time savings.

Using this FCM scheme, one can consider performing studies that were computationally prohibitive before. For instance, the analysis of the regioselectivities of all known clusters of the I_h-C_{80} cage using this method is underway in our group. Results from this study will be reported in due course.

ASSOCIATED CONTENT

Supporting Information

Full details of ref 20. Table S1 comparing energy barriers and reaction energies for all studied systems and Tables S2−S5 with actual and noncluster energy barriers and deformation energies for the cases not shown in the main paper, frozen cage model reaction energies obtained with single- and double-ζ basis sets, correlation coefficients and *p*-values obtained in multilinear regressions and plots of energy barriers, reaction energies, distortion energies, noncluster and noncluster with six electron energies, and frozen cage model energies for the cases not shown in the main paper. Figures S1−S5 with energy barriers, distortion energies, interaction energies, noncluster energies, and FCM energies for the cases not shown in the main paper. This material is available free of charge via the Internet at http://pubs.acs.org.

AUTHOR INFORMATION

Corresponding Author

*E-mail: josepm.luis@udg.edu (J.M.L.); marcel.swart@udg.edu(M.S.); miquel.sola@udg.edu (M.S.).

Notes

The authors declare no competing financial interest.

ACKNOWLEDGMENTS

The following organizations are thanked for financial support: the Ministerio de Ciencia e Innovación (MICINN, Project Nos. CTQ2011-25086/BQU and CTQ2011-23156), and the DIUE of the Generalitat de Catalunya (Project Nos. 2009SGR637 and 2009SGR528). M.G.-B. thanks the Spanish MEC for doctoral fellowship AP2010-2517. S.O. is grateful to the European Community for postdoctoral fellowship PIOF-GA-2009-252856. Excellent service by the Centre de Serveis Científic i Acadèmics de Catalunya (CESCA) is gratefully acknowledged. The authors also are grateful to the computer resources, technical expertise, and assistance provided by the Barcelona Supercomputing Center—Centro Nacional de Supercomputación. Support for the research of M.S. was received through the ICREA Academia 2009 prize for excellence in research funded by the DIUE of the Generalitat de Catalunya.

REFERENCES

(1) *Endofullerenes: A New Family of Carbon Cluster*; Akasaka, T., Nagase, S., Eds.; Kluwer: Dordrecht, The Netherlands, 2002. *Chemistry of Nanocarbons*; Akasaka, T., Wudl, F., Nagase, S., Eds.; John Wiley & Sons: Chichester, U.K., 2010. Liu, S.; Sun, S. *J. Organomet. Chem.* **2000**, *599*, 74. Dunsch, L.; Yang, S. *Small* **2007**, *3*, 1298. Yamada, M.; Akasaka, T.; Nagase, S. *Acc. Chem. Res.* **2010**, *43*, 92. Rodríguez-Fortea, A.; Balch, A. L.; Poblet, J. M. *Chem. Soc. Rev.* **2011**, *40*, 3551. Maeda, Y.; Tsuchiya, T.; Lu, X.; Takano, Y.; Akasaka, T.; Nagase, S. *Nanoscale* **2011**, *3*, 2421. Yang, S.; Liu, F.; Chen, C.; Jiao, M.; Wei, T. *Chem. Commun.* **2011**, *47*, 11822.

(2) Guha, S.; Nakamoto, K. *Coord. Chem. Rev.* **2005**, *249*, 1111.

(3) Chaur, M. N.; Melin, F.; Ortiz, A. L.; Echegoyen, L. *Angew. Chem., Int. Ed.* **2009**, *48*, 7514.

(4) Lu, X.; Akasaka, T.; Nagase, S. *Chem. Commun.* **2011**, *47*, 5942.

(5) Akasaka, T.; Kato, T.; Kobayashi, K.; Nagase, S.; Yamamoto, K.; Funasaka, H.; Takahashi, T. *Nature* **1995**, *374*, 600.

(6) Hirsch, A. *Angew. Chem., Int. Ed. Engl.* **1993**, *32*, 1138.

(7) Kareev, I. E.; Lebedkin, S. F.; Bubnov, V. P.; Yagubskii, E. B.; Ioffe, I. N.; Khavrel, P. A.; Kuvychko, I. V.; Strauss, S. H.; Boltalina, O. V. *Angew. Chem., Int. Ed.* **2005**, *44*, 1846.

(8) Osuna, S.; Rodríguez-Fortea, A.; Poblet, J. M.; Solà, M.; Swart, M. *Chem. Commun.* **2012**, *14*, 2486.

(9) Osuna, S.; Swart, M.; Solà, M. *Phys. Chem. Chem. Phys.* **2011**, *13*, 3585.
(10) Rodríguez-Fortea, A.; Irle, S.; Poblet, J. M. *WIREs Comput. Mol. Sci.* **2011**, *1*, 350. Osuna, S.; Swart, M.; Solà, M. In *Carbon Bonding and Structures: Advances in Physics and Chemistry*; Putz, M. V., Ed.; Springer: New York, 2011; p 57.
(11) Osuna, S.; Swart, M.; Campanera, J. M.; Poblet, J. M.; Solà, M. *J. Am. Chem. Soc.* **2008**, *130*, 6206.
(12) Osuna, S.; Swart, M.; Solà, M. *J. Am. Chem. Soc.* **2009**, *131*, 129.
(13) Garcia-Borràs, M.; Osuna, S.; Luis, J. M.; Swart, M.; Solà, M. *Chem.—Eur. J.* **2012**. DOI: 10.1002/chem.201103701.
(14) Campanera, J. M.; Bo, C.; Olmstead, M. M.; Balch, A. L.; Poblet, J. M. *J. Phys. Chem. A* **2002**, *106*, 12356.
(15) Osuna, S.; Swart, M.; Solà, M. *J. Phys. Chem. A* **2010**, *115*, 3491.
(16) Svensson, M.; Humbel, S.; Froese, R. D. J.; Matsubara, T.; Sieber, S.; Morokuma, K. *J. Phys. Chem.* **1996**, *100*, 19357. Dapprich, S.; Komáromi, I.; Byu, K. S.; Morokuma, K.; Frisch, M. J. *J. Mol. Struct. (THEOCHEM)* **1999**, *461−462*, 1.
(17) Osuna, S.; Morera, J.; Cases, M.; Morokuma, K.; Solà, M. *J. Phys. Chem. A* **2009**, *113*, 9721.
(18) Dimroth, O. *Angew. Chem.* **1933**, *46*, 571.
(19) te Velde, G.; Bickelhaupt, F. M.; Baerends, E. J.; Fonseca Guerra, C.; van Gisbergen, S. J. A.; Snijders, J. G.; Ziegler, T. *J. Comput. Chem.* **2001**, *22*, 931.
(20) Baerends, E. J.; et al. *ADF2010.01*; SCM: Amsterdam, 2010.
(21) Baerends, E. J.; Ellis, D. E.; Ros, P. *Chem. Phys.* **1973**, *2*, 41.
(22) Vosko, S. H.; Wilk, L.; Nusair, M. *Can. J. Phys.* **1980**, *58*, 1200.
(23) Becke, A. D. *Phys. Rev. A* **1988**, *38*, 3098.
(24) Perdew, J. P. *Phys. Rev. B* **1986**, *33*, 8822.
(25) van Lenthe, E.; Baerends, E. J.; Snijders, J. G. *J. Chem. Phys.* **1993**, *99*, 4597.
(26) Swart, M.; Bickelhaupt, F. M. *J. Comput. Chem.* **2008**, *29*, 724.
(27) Swart, M.; Bickelhaupt, F. M. *Int. J. Quantum Chem.* **2006**, *106*, 2536.
(28) Kroto, H. W. *Nature* **1987**, *329*, 529.
(29) Marcus, R. A. *J. Chem. Phys.* **1956**, *24*, 966.
(30) Marcus, R. A. *Pure Appl. Chem.* **1997**, *69*, 13.
(31) Koeppl, G. W.; Kresge, A. J. *J. Chem. Soc., Chem. Commun.* **1973**, 371.
(32) Evans, M. G.; Polanyi, M. *Trans. Faraday Soc.* **1938**, *34*, 11.
(33) Osuna, S.; Houk, K. N. *Chem.—Eur. J.* **2009**, *15*, 13219.
(34) Slanina, Z.; Stobinski, L.; Tomasik, P.; Lin, H.-M.; Adamowicze, L. *J. Nanosci. Nanotechnol.* **2003**, *3*, 193.
(35) Cui, Q.; Musaev, D. G.; Morokuma, K. *Organometallics* **1997**, *16*, 1355. Morokuma, K. *Acc. Chem. Res.* **1977**, *10*, 294. Zheng, G. S.; Wang, Z.; Irle, S.; Morokuma, K. *J. Am. Chem. Soc.* **2006**, *128*, 15117.
(36) Bickelhaupt, F. M. *J. Comput. Chem.* **1999**, *20*, 114.
(37) de Jong, G. T.; Bickelhaupt, F. M. *ChemPhysChem* **2007**, *8*, 1170. van Zeist, W.-J.; Bickelhaupt, F. M. *Org. Biomol. Chem.* **2010**, *8*, 3118. Fernández, I.; Bickelhaupt, F. M.; Cossío, F. P. *Chem.—Eur. J.* **2009**, *15*, 13022.
(38) Ess, D. H.; Houk, K. N. *J. Am. Chem. Soc.* **2007**, *129*, 10646. Ess, D. H.; Houk, K. N. *J. Am. Chem. Soc.* **2008**, *130*, 10187.
(39) Campanera, J. M.; Bo, C.; Poblet, J. M. *Angew. Chem., Int. Ed.* **2005**, *44*, 7230. Chaur, M. N.; Valencia, R.; Rodríguez-Fortea, A.; Poblet, J. M.; Echegoyen, L. *Angew. Chem., Int. Ed.* **2009**, *48*, 1425.
(40) Rodríguez-Fortea, A.; Alegret, N.; Balch, A. L.; Poblet, J. M. *Nat. Chem.* **2010**, *2*, 955.